

# THE EFFECTS OF ENGINE MASS AND LOCATION ON THE FLUTTER CHARACTERISTICS OF AIRCRAFT WINGS

J. Ranjan Banerjee<sup>1</sup>, Ajandan Ananthapuvirajah<sup>1</sup> & Pedro Higino Cabral<sup>2</sup>

<sup>1</sup>Department of Mechanical Engineering and Aeronautics, School of Science and Technology City, University of London, Northampton Square, London EC1V 0HB, United Kingdom

<sup>2</sup>Department of Technology Development (Aeronautics), Embraer S.A. Sao Jose dos Campos, SP-Brazil

#### **Abstract**

The effects of engine mass and location on the flutter characteristics of transport aircraft wings are investigated in this paper. Four representative transport aircraft wings are investigated for their flutter characteristics. This is achieved first by idealising the wing, structurally and aerodynamically. The structural idealisation includes a coupled bending-torsion beam element representation of the wing through the application of the dynamic stiffness method. To this end, the wing is modelled as a series of bending-torsion coupled beams connected at nodes. The aerodynamic idealisation is based on the two-dimensional unsteady aerodynamics theory given by Theodorsen, considering the spanwise variations of the wing chord. The free vibration or modal analysis is carried out using the dynamic stiffness method through the implementation of the Wittrick-Williams algorithm, as solution technique. This is followed by flutter analysis using the normal mode method in conjunction with the generalised co-ordinates. The complex flutter matrix is formed by summing the generalised mass, stiffness, and aerodynamic matrices. The flutter determinant is subsequently solved for flutter speed and flutter frequency, which is basically an iterative process in that the complex (double) eigenvalue problem involving both the airspeed and the frequency is handled. Thus, the computation is focused on the vanishing of both the real and imaginary parts of the flutter determinant for a particular airspeed and frequency which are the flutter speed and flutter frequency. The complete procedure for modal and flutter analyses of an aircraft wing is an integral part of the computer program CALFUN (CALculation of Flutter speed Using Normal modes) developed by the first author more than four decades ago. CALFUN has been successfully used on numerous occasions in the past to investigate the aeroelastic behaviour of aircraft wings. With this pretext, CALFUN has been used to analyse four representative transport aircraft wings in this paper, which are designated as T<sub>1</sub>, T<sub>2</sub>, T<sub>3</sub> and T<sub>4</sub>. Two of the aircraft carry one engine on each wing, while the other two carry two engines on each wing. The main purpose of this paper is to investigate the effects of the engine mass and location on the free vibration and flutter behaviour of the above four wings when a cantilever boundary condition is applied at the root. A detailed parametric investigation is carried out on these wide-ranging aircraft wings and the results are discussed with significant conclusions drawn. The findings of this research could be of great help to the aircraft industry.

Keywords: Aircraft wings; Flutter analysis; Dynamic stiffness method; Wittrick-Williams algorithm

#### 1. Introduction

Transport aircraft wings are generally slender because of their high aspect ratios ranging typically between 8 and 12. Consequently, they can be prone to flutter and other dynamic phenomena. In this respect, flutter analysis of transport aircraft wings, has always been an area of intense research activity. Furthermore, it is one of the mandatory airworthiness requirements to carry out flutter analysis of aircraft wings, as laid down by the aviation authorities. For high aspect ratio aircraft wings such as those of transport airliners the flutter behaviour is principally affected by, their bending (*EI*) and torsional stiffnesses (*GJ*) as well as by their mass and inertia distributions. Additionally, the engine masses and their locations on the wing can have significant effects on the flutter behaviour. The purpose of this paper is to carry out a detailed investigation on the effects of engine masses and their locations on flutter behaviour for a range of high aspect ratio transport aircraft wings using the normal mode method and generalised coordinates. The dynamic stiffness method is applied for the modal behaviour and Theodorsen type unsteady aerodynamics for the flutter behaviour.

There are several papers published in the literature dealing with the free vibration and flutter behaviour of hight aspect ratio aircraft, see for example [1-9]. In general, the finite element method (FEM) is widely used to investigate the modal and flutter behaviour of aircraft wings. When the normal mode method of flutter analysis is employed, the free vibration analysis is first carried out to generate the mode shapes and then, through the application of generalised coordinates, the flutter problem is formulated using some form of unsteady aerodynamics such as that of Theodorsen type [1, 2, 7, 9]. Thus, the free vibration or modal analysis is the first step prior to flutter analysis. In this respect, the FEM is commonly and routinely used. However, FEM is an approximate method based on assumed shaped functions from which the stiffness and mass properties of all individual elements are derived and assembled to form the overall stiffness matrix [K] and mass matrix [M] of the final structure, which in this case, is an aircraft wing. Next, the modal analysis is carried out by imposing the boundary conditions. The procedure in FEM leads to a linear eigenvalue problem of the type  $[[K] - \lambda[M]] \{\Delta\} = 0$  where  $\{\Delta\}$  is the nodal displacement vector and the square root of  $\lambda$  (the eigen parameter) gives the natural frequencies of the structure.

Against the above background, there is a powerful alternative to FEM for modal analysis of structures such as an aircraft wing. The alternative is that of the dynamic stiffness method (DSM) [10-12] which is not as widely used as the FEM. Notably, there are differences and similarities between FEM and the DSM. For instance, the DSM unlike the FEM, relies on only one frequency dependent dynamic stiffness element as the basic building block which contains both the mass and stiffness properties of the element in an exact sense because the shape function used in DSM is not assumed, but derived from the exact solution of the governing differential equation of the structural elements in free vibration. This is in sharp contrast to FEM which uses separate (frequency-independent) mass and stiffness matrices. The assembly procedure of structural elements in the DSM is essentially the same as the FEM, but the former unlike the latter, uses a single dynamic stiffness matrix element for each structural component as mentioned earlier to form the overall frequency-dependent dynamic stiffness matrix KD of the complete structure (wing). The eigenvalue problem in DSM is then expressed in the form  $[K_D]{\{\Delta\}} = 0$ where  $\{\Delta\}$  is the nodal displacement vector comprising amplitudes of nodal displacements. The next step in the DSM is to extract the natural frequencies of the structure by solving the above transcendental and non-linear eigenvalue problem. The best available solution technique to achieve this objective is to apply the Wittrick-Williams algorithm [13], which has featured in literally hundreds of papers. The algorithm monitors the Sturm sequence property of the dynamic stiffness matrix, and it ensures that no natural frequency of the structure is missed. Given the importance and effectiveness of this solution technique, the dynamic stiffness method and the Wittrick-Williams algorithm are somehow permanently intertwined with each together.

As stated earlier, in the structural idealisation of the wing, dynamic stiffness theory of a bending-torsion coupled beam is used to represent the wing [11,12] whereas in the aerodynamic idealisation strip theory based on Theodorsen type unsteady aerodynamics [14] is exploited in the flutter formulation. The computer program CALFUN [15] which was written using these established structural and aerodynamic theories, has been extensively used when obtaining the results for this paper.

The research is first focused on the modal analysis and then on flutter analysis. Four transport aircraft wings are analysed for both modal and flutter analysis. Bending and torsional stiffness properties and the details of the mass and inertia distributions were calculated from the original data for each aircraft wing, which required considerable time and efforts to input into CALFUN. Once the modelling and data preparation were completed for the respective wings, modal and flutter analysis were performed first on the original (unmodified) wing. Then, a detailed parametric study was undertaken by varying the engine mass and location to investigate the modal and flutter characteristics of each of the four wings. The values for the engine masses and their locations from the wing root were varied between +25% and -25% in steps of 5% and their subsequent effects on the modal and flutter behaviour were examined. The results showing interesting trends and possibilities are discussed and commented on. The paper concludes with significant remarks.

### 2. Dynamic Stiffness Method (DSM) for Free Vibration Analysis

The basic building block in DSM is the dynamic stiffness matrix of a structural element which essentially relates the amplitudes of the forces to those of the corresponding displacements at the nodes of the harmonically vibrating structural element. A general procedure to formulate the dynamic stiffness matrix of a structural element is briefly described in the following steps:

- (i) Derive the governing differential equation of motion in free vibration of the structural element for which the dynamic stiffness matrix is to be developed. This can be achieved by applying Newton's second law or Lagrange's equation or Hamilton's principle. However, Hamilton's principle is preferred because unlike Newton's second law and Lagrange's equation, the variationally based Hamilton's principle provides natural boundary conditions, giving the expressions for forces and moments which are required in the dynamic stiffness formulation.
- (ii) For harmonic oscillation, seek a closed form analytical solution of the governing differential equation derived in (i) above, in terms of the arbitrary integration constants. The number of constants in the general solution will, of course, depend on the order of the differential equation.
- (iii) Apply the boundary conditions in algebraic form. The number of boundary conditions is generally equal to twice the number of integration constants. The boundary conditions are typically the nodal displacements and forces.
- (iv) Eliminate the constants by relating the harmonically varying amplitudes of nodal forces to the corresponding displacements at the nodes of the element. This will generate the frequency dependent dynamic stiffness matrix connecting dynamically the amplitudes of the nodal forces to those of the nodal displacements.

# 2.1 Structural Idealisation of High Aspect Ratio Aircraft Wings Using the Dynamic Stiffness Method

An aircraft wing shown in Figure 1 is a classic example of a bending-torsion coupled beam. Such a representation is particularly relevant to analyse a high aspect ratio wing. A non-uniform aircraft wing can be modelled by assembling several uniform bending-torsion coupled beams such as the one shown in Figure 1. An important feature of the model both at an element level as well as at an assembly level is that the coupling between the bending and torsional deformations are clearly prevalent during the free vibratory motion.

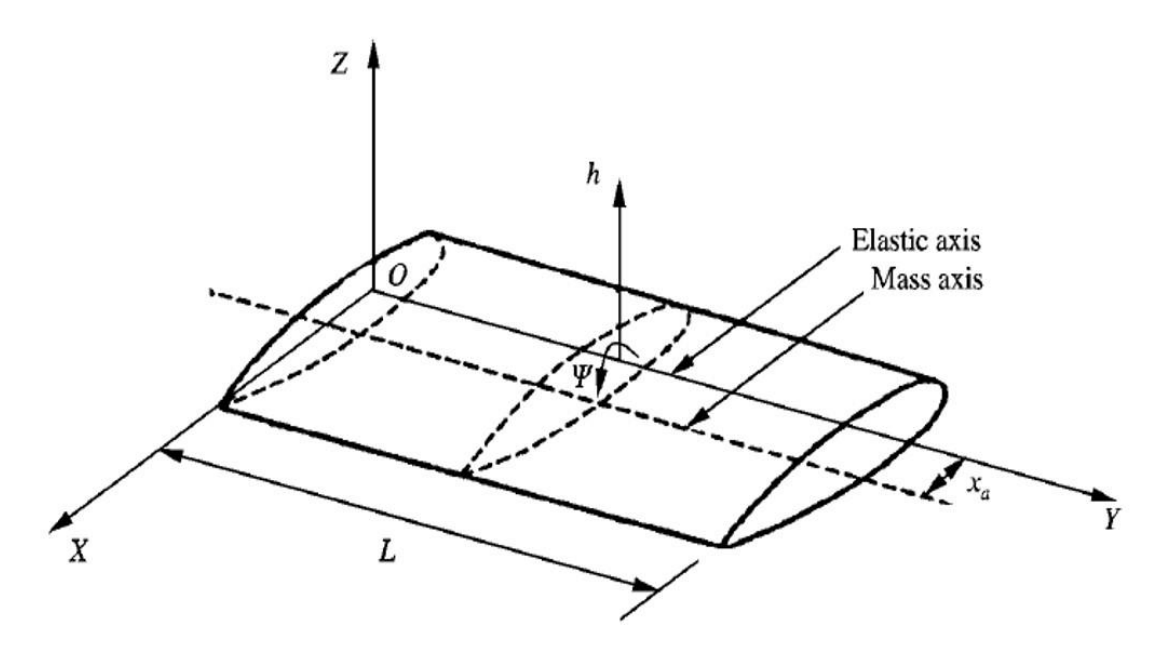


Figure 1 – An aircraft wing idealised as a bending-torsion coupled beam.

In essence, the coupling between the bending and the torsional motions arises due to non-coincident mass and elastic axes which are respectively the loci of the centroid and shear centres of the beam (wing) cross-section. Thus, for an aircraft wing it is not generally possible to realize a torsion-free bending displacement or a bending-free torsional rotation during the free vibratory motion. Given this perspective, this paper uses a dynamic stiffness approach and develops the dynamic stiffness matrix of a uniform bending-torsion coupled beam and then extends it to model a non-uniform aircraft wing.

The governing partial differential equations of motion of the bending-torsion coupled beam (wing) shown in Figure 1 are given by [11, 12]

$$EIh^{\prime\prime\prime\prime\prime} + m\ddot{h} - mx_{\alpha}\ddot{\psi} = 0 \tag{1}$$

$$GJ\psi^{\prime\prime} + mx_{\alpha}\ddot{h} - I_{\alpha}\ddot{\psi} = 0 \tag{2}$$

where EI and GJ are the bending and torsional stiffnesses of the beam, m is the mass per unit length,  $I_{\alpha}$  is the polar mass moment of inertia per length about the Y-axis,  $x_{\alpha}$  is the distance between the mass axis and the elastic axis, and a prime and an over-dot denote partial differentiation with respect to spanwise position y and time t, respectively.

For harmonic oscillation, sinusoidal variation in bending displacement h and torsional rotation  $\psi$  with circular or angular frequency  $\omega$  may be assumed to give

$$h(y,t) = H(y)\sin\omega t, \quad \psi(y,t) = \Psi(y)\sin\omega t \tag{3}$$

where H(y) and  $\Psi(y)$  denote the amplitude of the bending displacement and torsional rotation.

Substituting Equation (3) into Equations (1) and (2) eliminates the time component and gives the following ordinary differential equations

$$EIH^{\prime\prime\prime\prime} - m\omega^2 H + mx_{\alpha}\omega^2 \Psi = 0 \tag{4}$$

$$GJ\Psi'' + I_{\alpha}\omega^{2}\Psi - mx_{\alpha}\omega^{2}H = 0$$
(5)

where prime now denotes full differentiation with respect to y.

Equations (4) and (5) can be combined into a sixth order ordinary differential equation by eliminating either H or  $\Psi$  to give

$$W'''''' + \left(\frac{I_{\alpha}\omega^{2}}{GJ}\right)W'''' - \left(\frac{m\omega^{2}}{EI}\right)W''' - \left(\frac{m\omega^{2}}{EI}\right)\left(\frac{I_{\alpha}\omega^{2}}{GJ}\right)\left(\frac{I_{\alpha}-m\chi_{\alpha}^{2}}{I_{\alpha}}\right)W = 0$$
 (6)

where

$$W = H \text{ or } \Psi \tag{7}$$

Equation (6) can be non-dimensionalised by using the non-dimensional length  $\xi$  given by

$$\xi = \frac{y}{L} \tag{8}$$

Thus, with the help of Equation (8), the non-dimensional form of Equation (6) becomes

$$(D^6 + aD^4 - bD^2 - abc)W = 0 (9)$$

where a, b and c are non-dimensional parameters given by

$$a = \left(\frac{I_{\alpha}\omega^{2}L^{2}}{GJ}\right), \quad b = \left(\frac{m\omega^{2}L^{4}}{EI}\right), \quad c = \left(\frac{I_{\alpha}-mx_{\alpha}^{2}}{I_{\alpha}}\right)$$
 (10)

and D is the following differential operator

$$D = \frac{d}{d\xi} \tag{11}$$

The differential equation given by Equation (9) can be solved using standard procedures [11,12] to give

$$W(\xi) = C_1 \cosh \alpha \xi + C_2 \sinh \alpha \xi + C_3 \cos \beta \xi + C_4 \sin \beta \xi + C_5 \cos \gamma \xi + C_6 \sin \gamma \xi \tag{12}$$

where

$$\alpha = \left[ 2\left(\frac{q}{3}\right)^{\frac{1}{2}}\cos\left(\frac{\phi}{3}\right) - \frac{a}{3} \right]^{\frac{1}{2}}, \ \beta = \left[ 2\left(\frac{q}{3}\right)^{\frac{1}{2}}\cos\left(\frac{(\pi-\phi)}{3}\right) + \frac{a}{3} \right]^{\frac{1}{2}}, \ \gamma = \left[ 2\left(\frac{q}{3}\right)^{\frac{1}{2}}\cos\left(\frac{(\pi+\phi)}{3}\right) + \frac{a}{3} \right]^{\frac{1}{2}}$$
(13)

with

$$q = b + \frac{a^2}{3} \tag{14}$$

and

$$\phi = \cos^{-1} \left[ \frac{27abc - 9ab - 2a^3}{\left\{ 2(a^2 + 3b)^{\frac{3}{2}} \right\}} \right]$$
 (15)

In Equation (12),  $C_1$ – $C_6$  are the integration constants resulting from the solution of the governing differential equation (9).

 $W(\xi)$  in Equation (12) gives the solution for both the bending displacement H and the torsional rotation  $\Psi$ , but with two different sets of constants. Thus, we can write,

$$H(\xi) = A_1 \cosh \alpha \xi + A_2 \sinh \alpha \xi + A_3 \cos \beta \xi + A_4 \sin \beta \xi + A_5 \cos \gamma \xi + A_6 \sin \gamma \xi \tag{16}$$

and

$$\Psi(\xi) = B_1 \cosh \alpha \xi + B_2 \sinh \alpha \xi + B_3 \cos \beta \xi + B_4 \sin \beta \xi + B_5 \cos \gamma \xi + B_6 \sin \gamma \xi \tag{17}$$

The two different sets of constants  $A_1$ – $A_6$  and  $B_1$ – $B_6$  in Equations (16) and (17) can be related with the help of either Equation (4) or Equation (5) to give.

$$B_1 = k_{\alpha} A_1, \quad B_2 = k_{\alpha} A_2, \quad B_3 = k_{\beta} A_3, \quad B_4 = k_{\beta} A_4, \quad B_5 = k_{\gamma} A_5, \quad B_6 = k_{\gamma} A_6$$
 (18)

where

$$k_{\alpha} = \frac{b - \alpha^4}{b x_{\alpha}}, \quad k_{\beta} = \frac{b - \beta^4}{b x_{\alpha}}, \quad k_{\gamma} = \frac{b - \gamma^4}{b x_{\alpha}}$$
 (19)

The expressions for bending rotation  $\Theta(\xi)$ , bending moment  $M(\xi)$ , shear force  $S(\xi)$  and torque  $T(\xi)$  are given by

$$\Theta(\xi) = \left(\frac{1}{L}\right) H'(\xi) = \left(\frac{1}{L}\right) \{A_1 \alpha \sinh \alpha \xi + A_2 \alpha \cosh \alpha \xi - A_3 \beta \sin \beta \xi + A_4 \beta \cos \beta \xi - A_5 \gamma \sin \gamma \xi + A_6 \gamma \cos \gamma \xi\}$$
(20)

$$M(\xi) = -\left(\frac{EI}{L^2}\right)H''(\xi) = -\left(\frac{EI}{L^2}\right)\left\{A_1\alpha^2\cosh\alpha\xi + A_2\alpha^2\sinh\alpha\xi - A_3\beta^2\cos\beta\xi - A_4\beta^2\sin\beta\xi - A_5\gamma^2\cos\gamma\xi - A_6\gamma^2\sin\gamma\xi\right\}$$
(21)

$$S(\xi) = \left(\frac{EI}{L^3}\right) \{A_1 \alpha^3 \sinh \alpha \xi + A_2 \alpha^3 \cosh \alpha \xi + A_3 \beta^3 \sin \beta \xi - A_4 \beta^3 \cos \beta \xi + A_5 \gamma^3 \sin \gamma \xi - A_6 \gamma^3 \cos \gamma \xi\}$$
(22)

$$T(\xi) = \left(\frac{GJ}{L}\right)\Psi'(\xi) = \left(\frac{GJ}{L}\right)\{B_1\alpha \sinh \alpha\xi + B_2\alpha \cosh \alpha\xi - B_3\beta \sin \beta\xi + B_4\beta \cos \beta\xi - B_5\gamma \sin \gamma\xi + B_6\gamma \cos \gamma\xi\}$$
(23)

With the help of Equations (16) - (23), the dynamic stiffness matrix of the coupled bending-torsion beam element which is essentially an aircraft wing element can be developed by applying the boundary conditions algebraically for displacements and forces at the ends of the elements.

Referring to Figure 2, the boundary conditions for displacements are

At 
$$y = 0$$
  $(\xi = 0)$ :  $H = H_1$ ,  $\Theta = \Theta_1$  and  $\Psi = \Psi_1$  (24)

At 
$$y = L$$
  $(\xi = 1)$ :  $H = H_2$ ,  $\Theta = \Theta_2$  and  $\Psi = \Psi_2$ 

Similarly, referring to Figure 3, the boundary conditions for the forces are

At 
$$y = 0$$
  $(\xi = 0)$ :  $S = S_1$ ,  $M = M_1$  and  $T = -T_1$  (25)

At 
$$y = L$$
  $(\xi = 1)$ :  $S = -S_2$ ,  $M = -M_2$  and  $T = T_2$ 

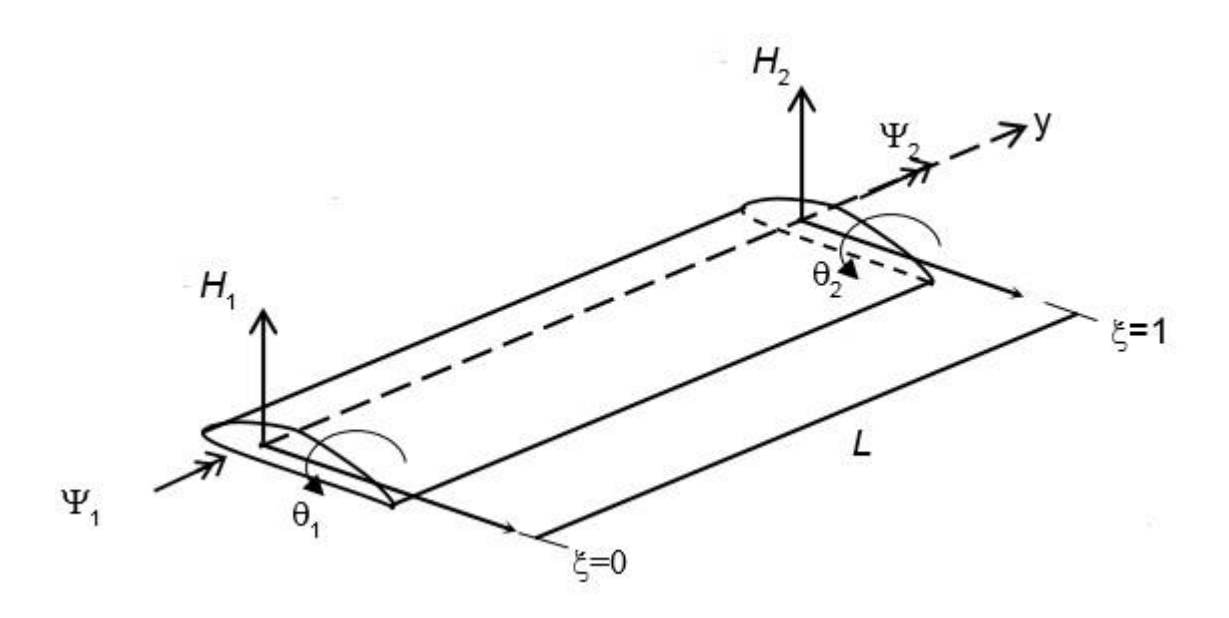


Figure 2 – Boundary conditions for displacements of an aircraft wing element.

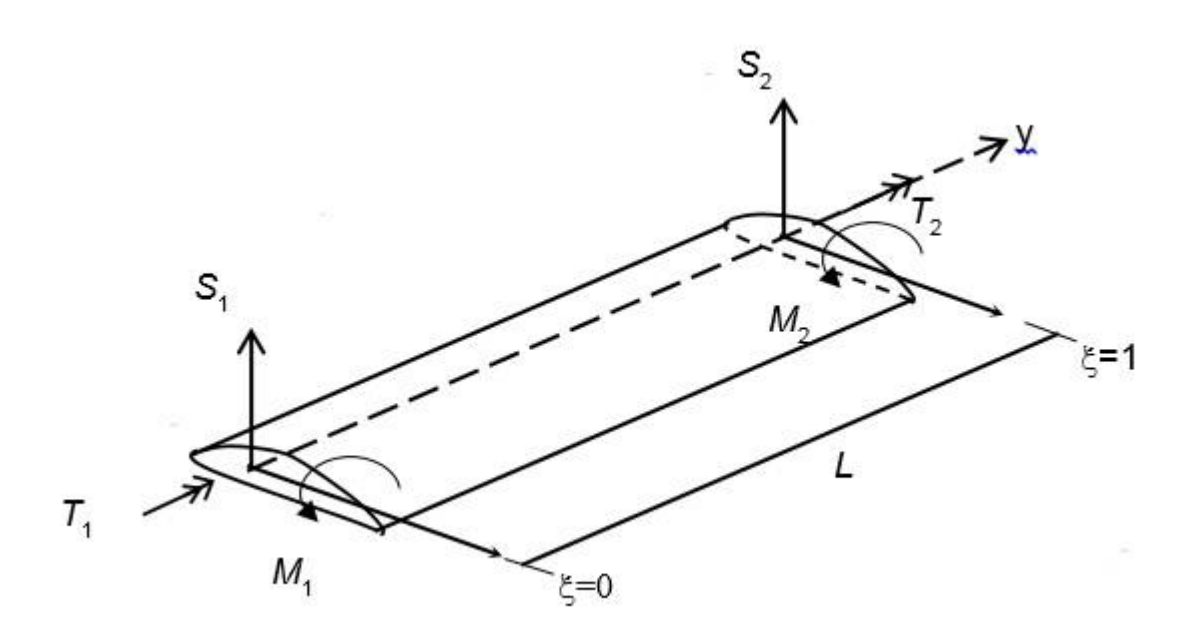


Figure 3 – Boundary conditions for forces of an aircraft wing element. Substituting the boundary conditions for displacements given by Equation (24) into Equations. (16), (17) and (19), one obtains the following matrix relationship.

$$\begin{bmatrix}
H_{1} \\
\Theta_{1} \\
\Psi_{1} \\
H_{2} \\
\Theta_{2} \\
\Psi_{2}
\end{bmatrix} = \begin{bmatrix}
1 & 0 & 1 & 0 & 1 & 0 \\
0 & \frac{\alpha}{L} & 0 & \frac{\beta}{L} & 0 & \frac{\gamma}{L} \\
k_{\alpha} & 0 & k_{\beta} & 0 & k_{\gamma} & 0 \\
k_{\alpha} & 0 & k_{\beta} & 0 & k_{\gamma} & 0 \\
C_{h_{\alpha}} & S_{h_{\alpha}} & C_{\beta} & S_{\beta} & C_{\gamma} & S_{\gamma} \\
\frac{\alpha}{L} S_{h_{\alpha}} & \frac{\alpha}{L} C_{h_{\alpha}} & -\frac{\beta}{L} S_{\beta} & \frac{\beta}{L} C_{\beta} & -\frac{\gamma}{L} S_{\gamma} & \frac{\gamma}{L} C_{\gamma} \\
k_{\alpha} C_{h_{\alpha}} & k_{\alpha} S_{h_{\alpha}} & k_{\beta} C_{\beta} & k_{\beta} S_{\beta} & k_{\gamma} C_{\gamma} & k_{\gamma} S_{\gamma}
\end{bmatrix} \begin{bmatrix} A_{1} \\ A_{2} \\ A_{3} \\ A_{4} \\ A_{5} \\ A_{6} \end{bmatrix}$$
(26)

or

$$\Delta = \mathbf{B}\mathbf{A} \tag{27}$$

where **A** is the contact vector comprising the constants  $A_1$ – $A_6$  and

$$C_{h_{\alpha}} = \cosh \alpha$$
;  $S_{h_{\alpha}} = \sinh \alpha$ ;  $C_{\beta} = \cos \beta$ ;  $S_{\beta} = \sin \beta$ ;  $C_{\gamma} = \cos \gamma$ ;  $S_{\gamma} = \sin \gamma$  (28)

Substituting the boundary conditions for forces given by Equation (25) into Equations (21), (22) and (23), one obtains the following matrix relationship.

$$\begin{bmatrix} S_{1} \\ M_{1} \\ T_{1} \\ S_{2} \\ M_{2} \\ T_{2} \end{bmatrix} = \begin{bmatrix} 0 & W_{3}\alpha^{3} & 0 & -W_{3}\beta^{3} & 0 & -W_{3}\gamma^{3} \\ -W_{2}\alpha^{2} & 0 & W_{2}\beta^{2} & 0 & W_{2}\gamma^{2} & 0 \\ 0 & -W_{1}k_{\alpha}\alpha & 0 & -W_{1}k_{\beta}\beta & 0 & -W_{1}k_{\gamma}\gamma \\ -W_{3}\alpha^{3}S_{h_{\alpha}} & -W_{3}\alpha^{3}C_{h_{\alpha}} & -W_{3}\beta^{3}S_{\beta} & W_{3}\beta^{3}C_{\beta} & -W_{3}\gamma^{3}S_{\gamma} & W_{3}\gamma^{3}C_{\gamma} \\ W_{2}\alpha^{2}C_{h_{\alpha}} & W_{2}\alpha^{2}S_{h_{\alpha}} & -W_{2}\beta^{2}C_{\beta} & -W_{2}\beta^{2}S_{\beta} & -W_{2}\gamma^{2}C_{\gamma} & -W_{2}\gamma^{2}S_{\gamma} \\ W_{1}k_{\alpha}\alpha S_{h_{\alpha}} & W_{1}k_{\alpha}\alpha C_{h_{\alpha}} & -W_{1}k_{\beta}\beta S_{\beta} & W_{1}k_{\beta}\beta C_{\beta} & -W_{1}k_{\gamma}\gamma S_{\gamma} & W_{1}k_{\gamma}\gamma C_{\gamma} \end{bmatrix} \begin{bmatrix} A_{1} \\ A_{2} \\ A_{3} \\ A_{4} \\ A_{5} \\ A_{6} \end{bmatrix}$$

$$(29)$$

or

$$\mathbf{F} = \mathbf{D}\mathbf{A} \tag{30}$$

where

$$W_1 = \frac{GJ}{L}; \ W_2 = \frac{EI}{L^2}; \ W_3 = \frac{EI}{L^3}$$
 (31)

The constant vector **A** can now be eliminated from Equations (27) and (30) to give the following force-displacement relationship

$$\mathbf{F} = \mathbf{K}\Delta \tag{32}$$

where **K** is the 6 x 6 frequency dependent dynamic stiffness matrix given by

$$\mathbf{K} = \mathbf{D}\mathbf{B}^{-1} \tag{33}$$

The dynamic stiffness matrix of Equation (33) representing a bending-torsion coupled beam can now be used to model an aircraft wing. A non-uniform aircraft wing can be modelled as an assembly of many uniform dynamic stiffness elements. For instance, the cantilever wing of Figure 4 can be modelled as a stepped cantilever beam (wing) as shown in Figure 5 where the non-uniform wing is split into typically 9 uniform dynamic stiffness elements. The dynamic stiffness elements of each of the 9 elements can

be assembled to form the overall dynamic stiffness matrix of the complete wing. Note that the theory given above is sufficiently general to handle swept wings with complex geometries.

The solution procedure to extract the natural frequencies and mode shapes from the overall dynamic stiffness matrix of the wing is based on the application of the Wittrick-Williams algorithm [13] as mentioned before. The algorithm is particularly suitable for solving free vibration problem using the dynamic stiffness method.

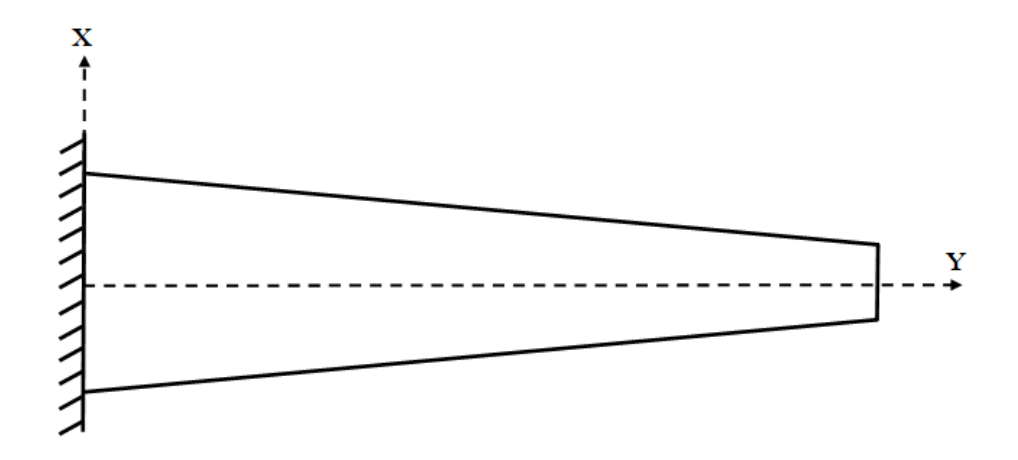


Figure 4 – A non-uniform cantilever wing.

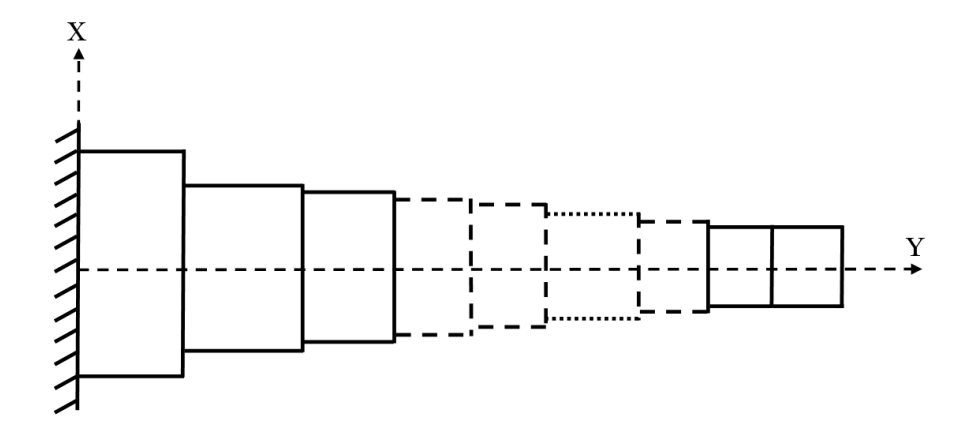


Figure 5 – A non-uniform cantilever wing idealised as a stepped beam.

## 2.2 Application of the Wittrick-Williams Algorithm

The dynamic stiffness matrix of Equation (34) can now be used to compute the natural frequencies and mode shapes of aircraft wings. A non-uniform and/or swept wing can be analysed for its natural frequencies and mode shapes by idealising it as an assemblage of many uniform dynamic stiffness elements of bending-torsion coupled beams. The natural frequency calculation is accomplished by applying the Wittrick-Williams algorithm [13] which has received extensive coverage in the literature. Before applying the algorithm, the dynamic stiffness matrices of all individual elements (see Figures 4 and 5) need to be assembled to form the overall dynamic stiffness matrix  $\mathbf{K}_{\mathrm{f}}$  of the final structure, i.e., the complete wing. The algorithm monitors the Sturm sequence condition of  $\mathbf{K}_{\mathrm{f}}$  in such a way that there is no possibility of missing any natural frequency of the wing. The application procedure of the algorithm is briefly summarised as follows.

Suppose that  $\omega$  denotes the circular (or angular) frequency of the vibrating wing. Then according to the Wittrick-Williams algorithm [13], j, the number of natural frequencies passed, as  $\omega$  is increased from zero to a trial frequency  $\omega^*$ , is given by

$$j = j_0 + s\{K_f\} \tag{34}$$

where  $\mathbf{K}_{\mathbf{f}}$ , the overall dynamic stiffness matrix of the wing whose elements depend on  $\omega$  is evaluated at  $\omega = \omega^*$ ;  $s\{K_f\}$  is the number of negative elements on the leading diagonal of  $K_f^{\Delta}$ ,  $K_f^{\Delta}$  is the upper triangular matrix obtained by applying the usual form of Gauss elimination to  $\mathbf{K}_{\mathbf{f}}$ , and  $j_0$  is the number of natural frequencies of the wing still lying between  $\omega = 0$ ; and  $\omega = \omega^*$ ; when the displacement components to which  $\mathbf{K}_{\mathbf{f}}$  corresponds are all zeros. (Note that the structure can still have natural frequencies when all its nodes are clamped, because exact member equations allow each individual member to displace with an infinite number of degrees of freedom, between nodes.) Thus

$$j_0 = \sum j_m \tag{35}$$

where  $j_m$  is the number of natural frequencies between  $\omega=0$  and  $\omega=\omega^*$  for an individual component member with its ends fully clamped, while the summation extends over all members of the structure. Thus, with the knowledge of Equations (34) and (35), it is possible to ascertain how many natural frequencies of the wing lie below an arbitrarily chosen trial frequency. This simple feature of the algorithm can be used to converge upon any required natural frequency to any desired accuracy. As successive trial frequencies can be chosen, computer implementation of the algorithm is very simple. However, for a detailed understanding, readers are referred to the original work of Wittrick and Williams [13].

# 3. Unsteady Aerodynamic Theory of Theodorsen

The unsteady aerodynamic theory for flutter analysis used in this paper is that of Theodorsen [14] who gave the expressions for the unsteady lift and moment of a unit strip cut out from a two-dimensional aerofoil, oscillating harmonically, and exhibiting bending displacement and torsional rotation in an incompressible air flow (see Figure 6). In standard notation, the semi-chord of the aerofoil is b, i.e., the chord is c = 2b, the airspeed is U and the elastic axis is located at a distance  $a_h b$  behind the mid-chord, as shown in Figure 6. If the bending displacement of the elastic axis is  $he^{i\omega t}$ , and torsional rotation about the elastic is  $\psi e^{i\omega t}$  where h and  $\psi$  are the amplitudes of bending displacement and torsional rotation,  $\omega$  being the circular or angular frequency of oscillation and  $i = \sqrt{-1}$ , then the expressions for the harmonically varying unsteady lift  $Le^{i\omega t}$  and moment  $Me^{i\omega t}$  are represented by the Theodorsen theory [14] as follows.

$$\frac{L}{\rho\pi bU^2} = -k^2 \left(\frac{h}{b} - a_h \psi\right) + ik\psi + 2C(k) \left\{\psi + \frac{i}{b}kh + \left(\frac{1}{2} - a_h\right)ik\psi\right\} \tag{36}$$

$$\frac{M}{\rho\pi b^2 U^2} = \left(\frac{1}{2} + a_h\right) 2C(k) \left\{\psi + \frac{i}{b}kh + \left(\frac{1}{2} - a_h\right)ik\psi\right\} - k^2 a_h \left(\frac{h}{b} - a_h\psi\right) - \left(\frac{1}{2} - a_h\right)ik\psi + \frac{k^2}{8}\psi$$
(37)

where k is the reduced frequency parameter and C(k) is the Theodorsen function given by

$$k = \frac{\omega b}{U};$$
  $C(k) = \frac{H_1^{(2)}(k)}{H_1^{(2)}(k) + iH_0^{(2)}(k)}$  (38)

In Equation (38),  $H_1^{(2)}(k)$  and  $H_0^{(2)}(k)$  are Hankel functions which are related to Bessel functions of first and second kinds and of orders 0 and 1, as follows.

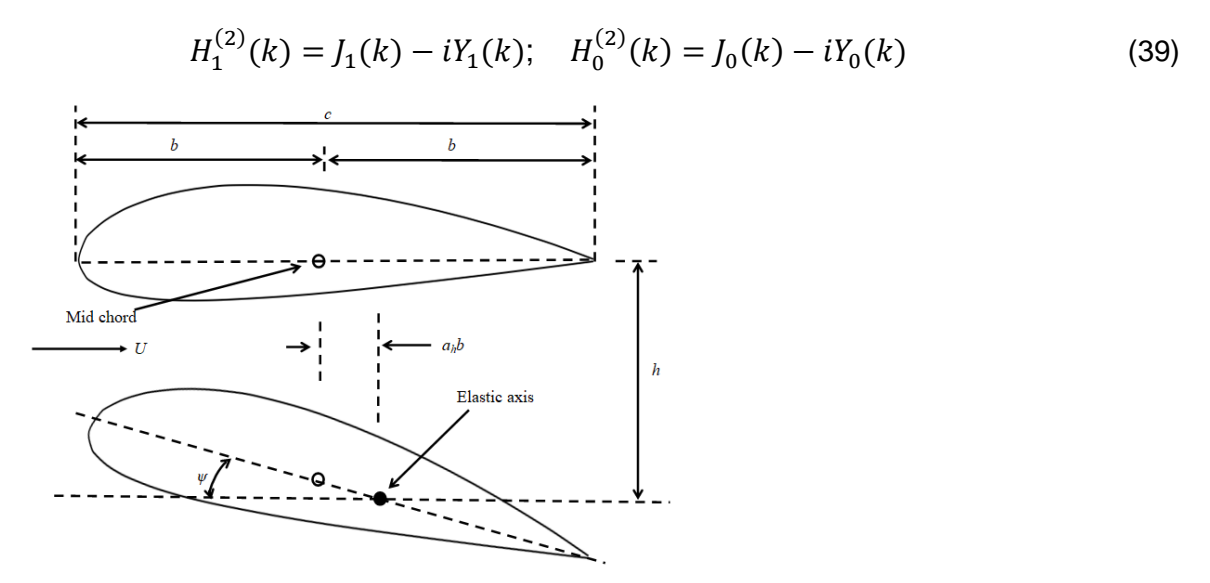


Figure 6 – A strip of unit width of a two-dimensional aerofoil with two degrees of freedom h and  $\psi$  in an incompressible airflow.

In the following section, the Theodorsen expressions for the unsteady lift and moment given in Equation (36) and (37) are integrated along the span, and subsequently applied in the formulation of the flutter problem.

# 4. Flutter Analysis Using Generalised Coordinates, Normal Modes, and Theodorsen Theory of Unsteady Aerodynamics

The normal mode method of flutter analysis is well known [1,2], particularly in the context of high aspect ratio wings for which the computer program CALFUN [15] is well suited (and it has a composite capability). CALFUN idealises the aircraft wing both structurally and aerodynamically. In the structural idealisation, bending-torsion coupled beam theory (the DSM method) is used to represent the wing [11,12] whereas the aerodynamic idealisation includes strip theory based on Theodorsen type unsteady aerodynamics [14]. The methodology is briefly summarised as follows.

## 4.1 Formulation of Generalised Mass and Stiffness Matrices

The mass and stiffness matrices of the wing are reduced to diagonal form to give generalised mass and stiffness matrices. This is achieved by using the normal modes obtained from the dynamic stiffness method. The procedure is briefly explained as follows.

If  $[\Phi]$  is the modal matrix, i.e., the matrix formed by the selected normal mode shapes so that each column of  $[\Phi]$  represents a normal mode shape  $\Phi_i$ , then the generalised mass and stiffness matrices are respectively obtained by post multiplying the mass and stiffness matrices by the modal matrix  $[\Phi]$ , and premultiplying the resultant matrix by the transpose of the modal matrix (i.e  $[\Phi]^T$ ). In matrix notation

$$[\mathbf{M}_{\mathbf{G}}] = [\Phi]^T [\mathbf{M}] [\Phi] \tag{40}$$

$$[\mathbf{K}_{\mathbf{G}}] = [\Phi]^T [\mathbf{K}] [\Phi] \tag{41}$$

where  $[\mathbf{M}_{\mathbf{G}}]$  and  $[\mathbf{K}_{\mathbf{G}}]$  are respectively, the generalised mass and stiffness matrices of the wing. Clearly if the number of modes chosen in the analysis is n, the order of  $[\mathbf{M}_{\mathbf{G}}]$  and  $[\mathbf{K}_{\mathbf{G}}]$  will each be of order  $n \times n$ .

## 4.2 Formulation of the Generalised Aerodynamic Matrix

The generalised aerodynamic matrix is formed by applying the principle of virtual work. The aerodynamic strip theory is based on Theodorsen's expressions for unsteady lift and moment [14] and the normal modes obtained from the dynamic stiffness method [11,12] are used when applying the principle of virtual work. The displacements considered are the vertical deflection (bending) h(y), and the pitching rotation (torsion)  $\Psi(y)$  of the elastic axis of the wing at a spanwise distance y from the root. Thus, the displacement components of the  $f^h$  mode  $\Phi_i$  are respectively,  $h_i(y)$  and  $\Psi_i(y)$ . If  $q_i(t)$  (i=1,2,3....n) are the generalised coordinates, then h(y) and  $\Psi(y)$  can be expressed as

$$h(y) = \sum_{i=1}^{n} h_i(y)q_i(t)$$
(42)

$$\Psi(y) = \sum_{i=1}^{n} \Psi_i(y) q_i(t)$$
(43)

Equations (42) and (43) can be written in the following matrix form

$$\begin{bmatrix} h(y) \\ \psi(y) \end{bmatrix} = \begin{bmatrix} h_1(y) & h_2(y) \cdots h_n(y) \\ \psi_1(y) & \psi_2(y) \cdots \psi_n(y) \end{bmatrix} \begin{bmatrix} q_1 \\ q_2 \\ \vdots \\ q_n \end{bmatrix}$$
(44)

If L(y) and M(y) are respectively the unsteady lift and moment at a spanwise distance y from the root, the virtual work done  $(\delta W)$  by the aerodynamic forces is given by

$$\delta W = \sum_{i=1}^{n} \delta q_i \int_0^s \{ L(y) h_i(y) + M(y) \Psi_i(y) \} dy$$
 (45)

where s is the semi-span of the wing and n is the number of normal modes considered in the analysis. Equation (45) can be written in matrix form as

$$\begin{bmatrix} \frac{\delta W_1}{\delta q_1} \\ \frac{\delta W_2}{\delta q_1} \\ \vdots \\ \frac{\delta W_n}{\delta q_n} \end{bmatrix} = \int_0^s \begin{bmatrix} h_1 & \psi_1 \\ h_2 & \psi_2 \\ \vdots & \vdots \\ h_n & \psi_n \end{bmatrix} \begin{bmatrix} L(y) \\ M(y) \end{bmatrix} dy \tag{46}$$

The unsteady lift L(y) and moment M(y) in two-dimensional flow given by Theodorsen [14] and shown by Equations (36) and (37) can be expressed in the following matrix form

where

$$A_{11} = -\pi \rho U^{2} \{-k^{2} + 2C(k)ik\}$$

$$A_{12} = -\pi \rho U^{2}b \left[ (a_{h}k^{2} + ik) + 2C(k) \left\{ 1 + ik \left( \frac{1}{2} - a_{h} \right) \right\} \right]$$

$$A_{21} = -\pi \rho U^{2}b \left\{ 2C(k)ik \left( \frac{1}{2} + a_{h} \right) - k^{2}a_{h} \right\}$$

$$A_{22} = -\pi \rho U^{2}b^{2} \left\{ 2\left( \frac{1}{2} + a_{h} \right)C(k) \left\{ 1 + ik \left( \frac{1}{2} - a_{h} \right) \right\} + \frac{k^{2}}{8} + k^{2}a_{h}^{2} + \left( a_{h} - \frac{1}{2} \right)ik \right\}$$

$$(48)$$

In the above equation, U, b,  $\rho$ , k, C(k) and  $a_h$  are in the usual notation: the airspeed, semi-chord, density of air, reduced frequency parameter, Theodorsen function and elastic axis location from mid-chord in non-dimensional form, respectively [14].

Substituting Equation (47) into Equation (46) and then using Equation (44) gives

$$\begin{vmatrix}
\frac{\partial H_1}{\partial q_1} \\
\frac{\partial W_2}{\partial q_1} \\
\vdots \\
\frac{\partial W_n}{\partial q_n}
\end{vmatrix} = \int_0^s \begin{bmatrix} h_1 & \psi_1 \\ h_2 & \psi_2 \\ \vdots & \vdots \\ h_n & \psi_n \end{bmatrix} \begin{bmatrix} A_{11} & A_{12} \\ A_{21} & A_{22} \end{bmatrix} \begin{bmatrix} h_1 & h_2 & \cdots & h_n \\ \psi_1 & \psi_2 & \cdots & \psi_n \end{bmatrix} \begin{bmatrix} q_1 \\ q_2 \\ \vdots \\ q_n \end{bmatrix} dy = \begin{bmatrix} QF_{11} & QF_{12} & \cdots & QF_{1n} \\ QF_{21} & QF_{22} & \cdots & QF_{2n} \\ \cdots & \cdots & \cdots & \cdots \\ QF_{n1} & QF_{n2} & \cdots & QF_{nn} \end{bmatrix} \begin{bmatrix} q_1 \\ q_2 \\ \vdots \\ q_n \end{bmatrix} \tag{49}$$

where [QF] is the generalised aerodynamics matrix with elements

$$QF_{ij} = \int_0^s (A_{11}h_ih_j + A_{12}h_i\Psi_i + A_{21}h_i\Psi_j + A_{22}\Psi_i\Psi_j) dy$$
 (50)

The generalised aerodynamic matrix  $[\mathbf{QF}]$  is usually a complex matrix with each element having a real part and an imaginary part. This is because the terms  $A_{11}, A_{12}, \ldots$  etc in Equation (50) are complex (see equations (48)). By contrast, the generalised mass and stiffness matrices are both real and diagonal matrices.

# 4.3 Formulation of Flutter Problem and Solution of the Flutter Determinant as a Double Eigenvalue Problem

The flutter determinant is the determinant formed from the flutter matrix which is formed by algebraically summing the generalised mass, stiffness, and aerodynamic matrices. Thus, for a system without structural damping (which generally has a small effect on the oscillatory motion and is not considered here) the flutter matrix [QA] can be formed as

$$[\mathbf{Q}\mathbf{A}]\{\mathbf{q}\} = [-\omega^2[\mathbf{M}_{\mathbf{G}}] + [\mathbf{K}_{\mathbf{G}}] - [\mathbf{Q}\mathbf{F}]]\{q\}$$
(51)

where  $\omega$  is the circular or angular frequency in rad/s of the oscillatory harmonic motion.

For the flutter condition to occur, the determinant of the complex flutter matrix must be zero so that from Equation (51),

$$\left|-\omega^{2}[\mathbf{M}_{\mathbf{G}}] + [\mathbf{K}_{\mathbf{G}}] - [\mathbf{Q}\mathbf{F}]\right| = 0 \tag{52}$$

The solution of the above flutter determinant is a complex eigenvalue problem because the determinant is primarily a complex function of two unknown variables, the airspeed (U) and the frequency ( $\omega$ ). The method used in CALFUN [15] selects an airspeed and evaluates the real and imaginary parts of flutter determinant for a range of frequencies and the process is repeated for a range of airspeeds, until both the real and imaginary parts of the flutter determinant (and hence the whole flutter determinant) vanish completely.

#### 5. Results

Using the above theory, four transport aircraft wings with cantilever boundary condition at the root are analysed for their flutter characteristics using the computer program CALFUN [15]. A typical layout of such aircraft is shown in Figure 7. Four wings of transport airliners (T<sub>1</sub>, T<sub>2</sub>, T<sub>3</sub> and T<sub>4</sub>) with particulars given in Table 1, are analysed.

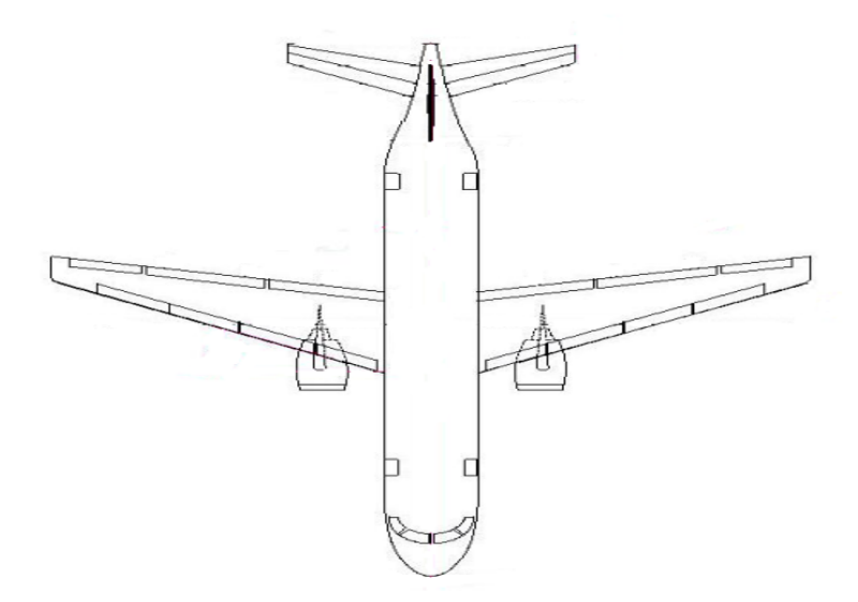
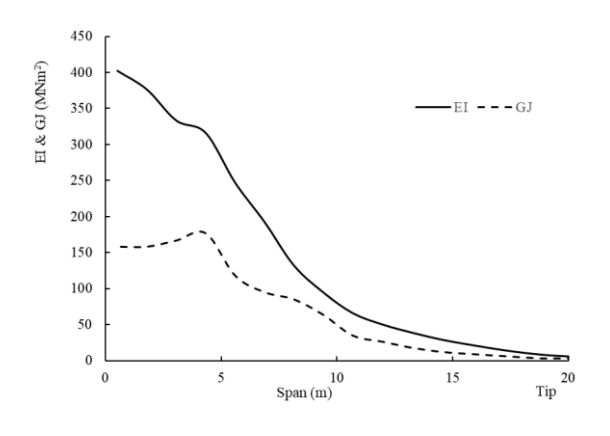


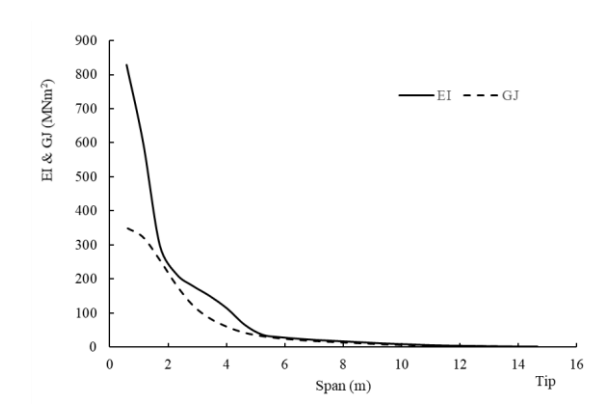
Figure 7 – A general lay-out of a typical transport aircraft.

Table 1 - Particulars of transport airliners

| B                           |                | Transpo        | ort airline           | r              |
|-----------------------------|----------------|----------------|-----------------------|----------------|
| Parameters                  | T <sub>1</sub> | T <sub>2</sub> | <b>T</b> <sub>3</sub> | T <sub>4</sub> |
| Wing Span (m)               | 40             | 30             | 35                    | 60             |
| Wing Area (m <sup>2</sup> ) | 162            | 93             | 123                   | 362            |
| Aspect Ratio                | 10             | 9              | 10                    | 10             |
| Wing Root Chord (m)         | 5              | 5.5            | 6                     | 10.5           |
| Wing Tip Chord (m)          | 2.5            | 1.5            | 1.5                   | 2.5            |
| Sweep Angle (deg)           | 0              | 28             | 28                    | 28             |
| Length Overall (m)          | 30             | 36             | 38                    | 60             |
| Height Overall (m)          | 12             | 11             | 12                    | 17             |
| Weight Empty (kg)           | 34000          | 26000          | 42000                 | 130000         |
| Max Take-off Weight (kg)    | 70000          | 46000          | 74000                 | 275000         |
| Max Wing Loading (kg/m²)    | 434            | 511            | 600                   | 760            |
| Max Cruising Speed (knots)  | 348            | 529            | 516                   | 569            |
| Range (nmi)                 | 2835           | 2400           | 2592                  | 8000           |
| Engine mass (kg)            | 3698           | 2827           | 4063                  | 7780           |
| Number of Engines           | 2              | 1              | 1                     | 2              |

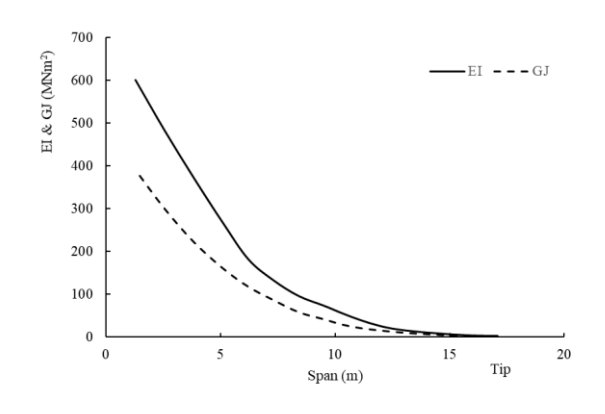
Figures 8-10 show the stiffness (bending stiffness EI and torsional stiffness GJ), mass per unit length and mass moment of inertia (MMOI) per unit length distributions of the transport aircraft wings  $T_1$ ,  $T_2$ ,  $T_3$  and  $T_4$ , respectively. These data were used to compute their natural frequencies and mode shapes. Figure 11 illustrates the first five natural frequencies and mode shapes of the  $T_1$ ,  $T_2$ ,  $T_3$  and  $T_4$  wings showing the bending displacements (solid lines) and torsional displacements (broken lines). For the  $T_1$  wing, the first two modes are bending modes, the third mode is coupled in bending and torsion, the fourth mode is bending, and the fifth mode is torsional. For the  $T_2$  wing, the first three modes are bending modes, while the fourth and fifth modes are coupled in bending and torsion. For the  $T_3$  wing, the first three modes are bending but the fourth and the fifth mode are essentially torsional. For the  $T_4$  wing, the first two and the fourth modes are bending dominated whereas the third and fifth modes are torsional.

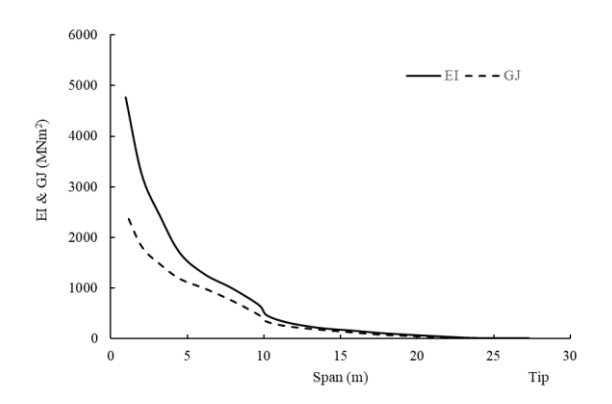




Stiffness distribution of transport airliner T<sub>1</sub>

Stiffness distribution of transport airliner T<sub>2</sub>

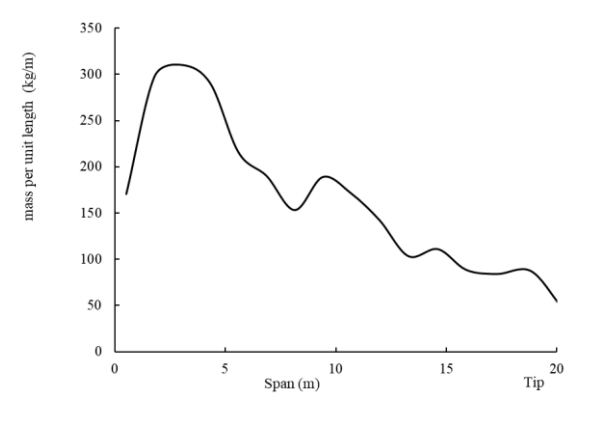


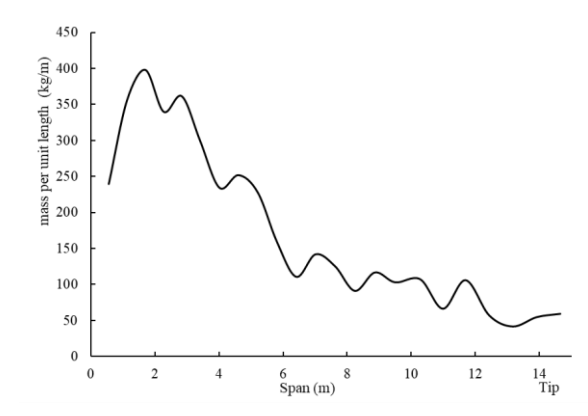


Stiffness distribution of transport airliner T<sub>3</sub>

Stiffness distribution of transport airliner T<sub>4</sub>

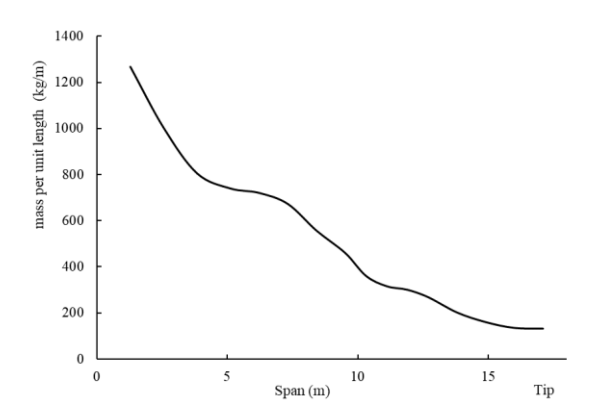
Figure 8 – Stiffness distributions of transport airliner wings.

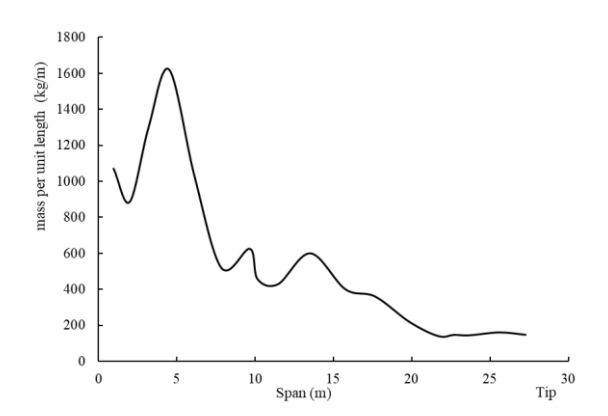




Mass per unit length variation of T<sub>1</sub>

Mass per unit length variation of T<sub>2</sub>





Mass per unit length variation of  $T_{\rm 3}$ 

Mass per unit length variation of T<sub>4</sub>

Figure 9 – Mass per unit length variation of transport airliner wings.

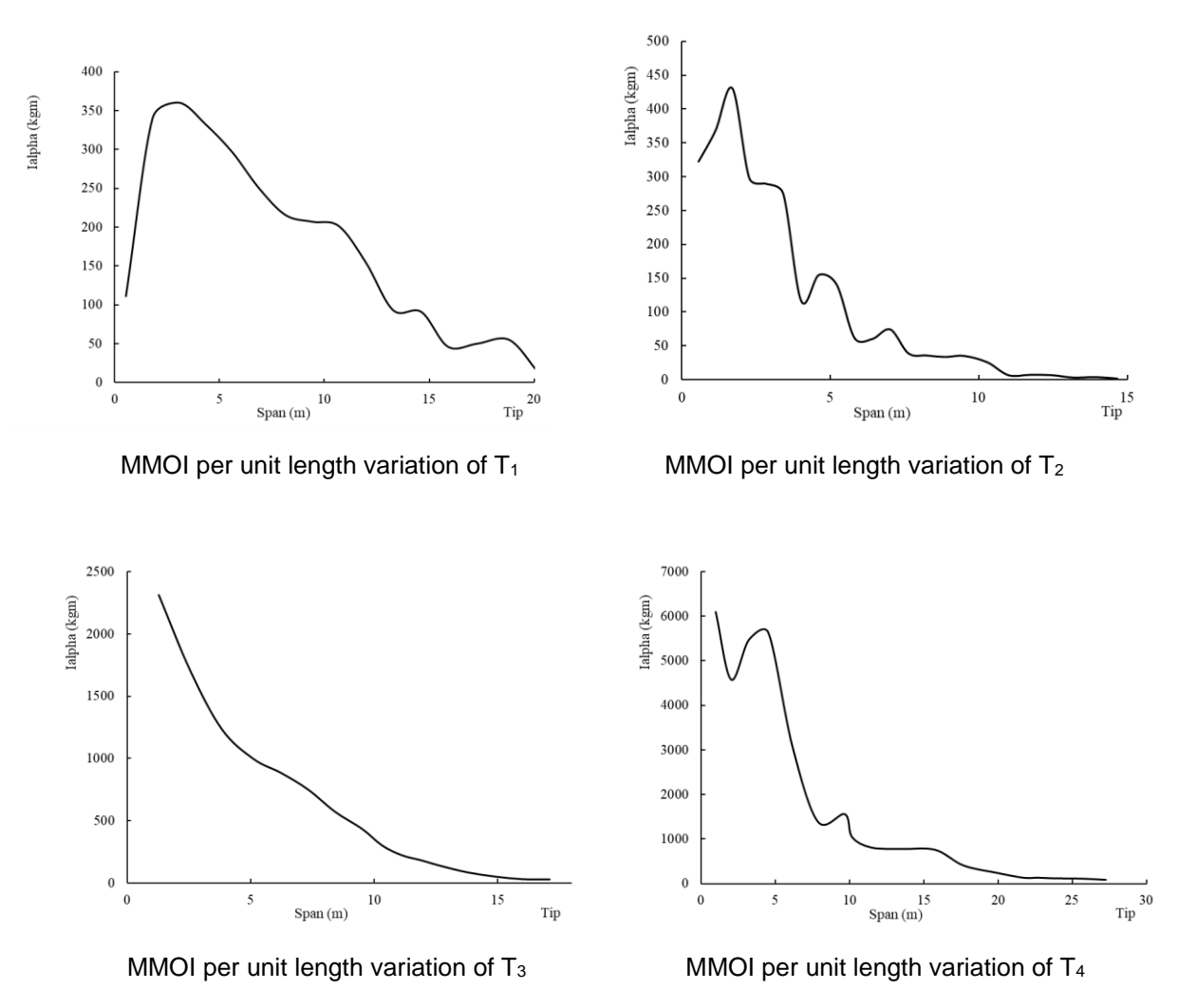


Figure 10 – Mass moment of inertia per unit length variation of transport airliner.

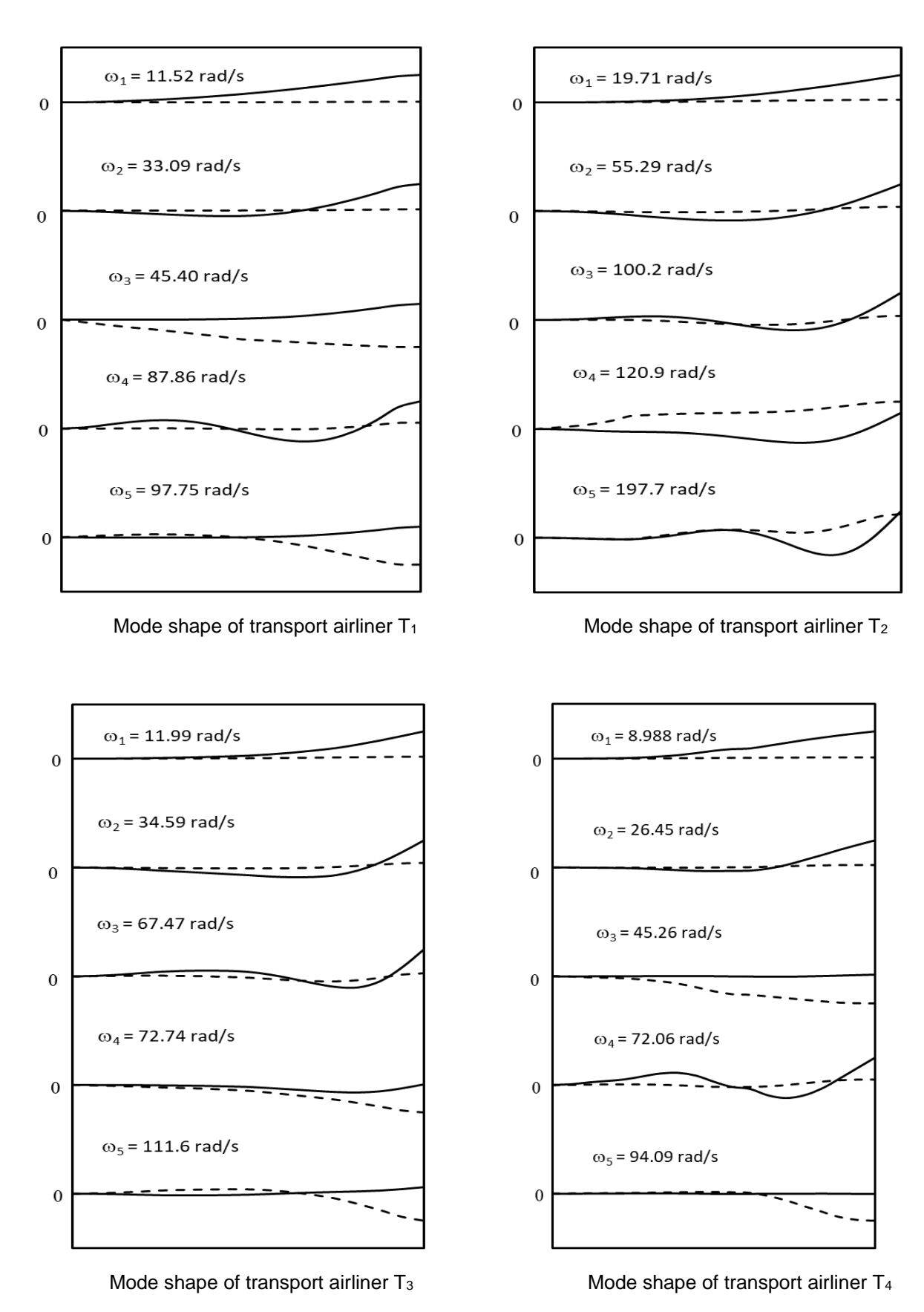


Figure 11 – Mode shapes of transport airliner.

The first five natural frequencies and flutter results for all of the original aircraft wings ( $T_1$ ,  $T_2$ ,  $T_3$  and  $T_4$ ) are given in Table 2. The letters B and T used in the table and elsewhere in the paper indicate bending and torsion dominated modes respectively whereas the letter C indicates a bending torsion coupled mode.

Table 2 - First five natural frequencies and flutter results of the baseline aircraft wings

|          |                       | Natural Fr            | equencies  | (ω <sub>i</sub> ) (rad/s) |                       | Flutter        | Flutter         |
|----------|-----------------------|-----------------------|------------|---------------------------|-----------------------|----------------|-----------------|
| Aircraft | <i>0</i> <sub>1</sub> | <i>0</i> <sub>2</sub> | <i>0</i> 3 | <i>0</i> 04               | <i>0</i> <sub>5</sub> | speed<br>(m/s) | freq<br>(rad/s) |
| T1       | 11.52 (B)             | 33.09 (B)             | 45.40 (C)  | 87.86 (B)                 | 97.75 (T)             | 249.1          | 28.77           |
| T2       | 19.71 (B)             | 55.29 (B)             | 100.3 (B)  | 120.9 (C)                 | 197.7 (C)             | 410.5          | 78.56           |
| Т3       | 11.99 (B)             | 34.59 (B)             | 67.47 (B)  | 72.74 (T)                 | 111.6 (T)             | 275.0          | 43.16           |
| T4       | 8.988 (B)             | 26.45 (B)             | 45.26 (T)  | 72.06 (B)                 | 94.09 (T)             | 385.8          | 46.50           |

A parametric study is now undertaken for all of the four transport airliner wings by varying the engine mass and location. It should be noted that among the four transport airliners,  $T_1$  and  $T_4$  have two engines on each of their wings, whereas  $T_2$  and  $T_3$ , each have a single engine on each of their wings. A variation between -25% to 25% in steps of 5% for the engine mass is allowed and for the engine locations, some realistic distances from the wing root relative to the current locations of the engines are considered. The first five natural frequencies with the identifications of the modes are presented in Tables 3 to 10 due to the engine mass and location variations. The results corresponding to the original engine mass and location of the baseline wing are shown in bold.

For the transport airliner T<sub>1</sub>, the first five natural frequencies due to the variation of engine masses and their locations are presented in Tables 3 and 4 respectively. It should be noted that the transport airliner T<sub>1</sub> has two engines on its wing and the masses of each of the two engines are both increased by the same amount as indicated in Table 3. Table 4 shows the results when the engine positions are changed for the T<sub>1</sub> wing. The outboard engine from its original location at 10.8m from the wing root was relocated in the analysis at 9.53m and 12.07m from the wing root, respectively whereas the original location of the inboard engine was altered from 5.59m to 4.32m and 6.93m, respectively. From the results shown in Tables 3 and 4, it can also be seen that the first, second and fourth modes are always bending while third mode is generally coupled in bending and torsion and the fifth mode is always torsional. For this wing, there is no significant change in the modal characteristics due to the variation of engine mass with the torsional natural frequency effectively unaltered, but the variation of engine location makes some difference in the natural frequencies, the maximum difference being around 10%. As expected, increasing engine mass reduces the natural frequencies particularly in bending, whereas reducing it, has the opposite effect. From Table 3, It can be observed that the flutter speed increases when the engine mass is increased. By contrast, the flutter speed decreases when the engine mass is decreased. The reason for this can be attributed to the fact that the separation between the fundamental bending and fundamental torsional natural frequencies increases when the engine mass is increased whereas the separation between the two frequencies decreases when the engine mass is reduced, bearing in mind that the fundamental bending and torsional modes are seen to be the main contributors to the flutter. Table 4 gives results showing the effects of engine location on the flutter of the T<sub>1</sub> wing, depicting a somewhat different picture. As expected, the outboard engine has a greater effect on the bending natural frequencies. This is principally due to the cantilever boundary condition assumption of the wing. The flutter speed of the T<sub>1</sub> wing is again influenced by the margin of separation between the fundamental bending and torsional natural frequencies in that, the greater the difference between the two frequencies, the greater the flutter speed and vice-versa. From the results shown in Tables 3 and 4, it is observed that around 5% change in the flutter speed is possible for the T1 wing. The flutter frequency lies between the fundamental bending and torsional natural frequencies. This is to be expected, particularly in classical bending-torsion flutter of a cantilever wing.

Table 3 – The effects of the variation of engine mass on the natural frequencies and flutter results of T<sub>1</sub> wing

| Variation             |            |                       | ω₁ (rad/s)            |                       |            | Flutter Flutter |                 |  |  |
|-----------------------|------------|-----------------------|-----------------------|-----------------------|------------|-----------------|-----------------|--|--|
| in Engine<br>mass (%) | <i>∞</i> ₁ | <i>w</i> <sub>2</sub> | <i>დ</i> <sub>3</sub> | <i>O</i> <sub>4</sub> | $\omega_5$ | speed<br>(m/s)  | freq<br>(rad/s) |  |  |
| -25                   | 11.97 (B)  | 34.55 (B)             | 45.40 (C)             | 92.02 (B)             | 97.76 (T)  | 237.0           | 30.63           |  |  |
| -20                   | 11.88 (B)  | 34.22 (B)             | 45.40 (C)             | 91.17 (B)             | 97.76 (T)  | 239.5           | 30.13           |  |  |
| -15                   | 11.79 (B)  | 33.91 (B)             | 45.40 (C)             | 90.32 (B)             | 97.75 (T)  | 241.5           | 29.87           |  |  |
| -10                   | 11.70 (B)  | 33.62 (B)             | 45.40 (C)             | 89.49 (B)             | 97.75 (T)  | 244.7           | 29.38           |  |  |
| -5                    | 11.61 (B)  | 33.35 (B)             | 45.40 (C)             | 88.67 (B)             | 97.75 (T)  | 248.0           | 29.08           |  |  |
| 0                     | 11.52 (B)  | 33.09 (B)             | 45.40 (C)             | 87.86 (B)             | 97.75 (T)  | 249.0           | 28.77           |  |  |
| 5                     | 11.44 (B)  | 32.84 (B)             | 45.40 (C)             | 87.07 (B)             | 97.75 (T)  | 250.5           | 28.44           |  |  |
| 10                    | 11.36 (B)  | 32.61 (B)             | 45.40 (C)             | 86.28 (B)             | 97.75 (T)  | 254.6           | 28.05           |  |  |
| 15                    | 11.28 (B)  | 32.39 (B)             | 45.40 (C)             | 86.28 (B)             | 97.75 (T)  | 255.5           | 27.63           |  |  |
| 20                    | 11.20 (B)  | 32.17 (B)             | 45.40 (C)             | 86.28 (B)             | 97.75 (T)  | 256.0           | 27.37           |  |  |
| 25                    | 11.12 (B)  | 31.97 (B)             | 45.39 (C)             | 84.01 (B)             | 97.74 (T)  | 258.5           | 26.88           |  |  |

Table 4 – The effects of the variation of engine location on the natural frequencies and flutter results of T<sub>1</sub>

| Engine<br>1 from    | Engine<br>2 from    |            |            |            | Flutter    | Flutter    |                |                 |
|---------------------|---------------------|------------|------------|------------|------------|------------|----------------|-----------------|
| wing<br>root<br>(m) | wing<br>root<br>(m) | <i>©</i> 1 | <i>∞</i> 2 | <i>დ</i> 3 | <i>©</i> 4 | <i>0</i> 5 | speed<br>(m/s) | freq<br>(rad/s) |
| 12.07               | 5.59                | 10.73 (B)  | 34.40 (B)  | 42.45 (C)  | 79.79 (B)  | 92.83 (T)  | 254.2          | 27.62           |
| 12.07               | 4.32                | 10.80 (B)  | 35.10 (B)  | 42.96 (C)  | 86.25 (B)  | 95.67 (T)  | 256.0          | 27.92           |
| 10.80               | 6.93                | 11.36 (B)  | 32.13 (B)  | 44.05 (C)  | 86.87 (B)  | 97.10 (T)  | 252.0          | 28.84           |
| 10.80               | 5.59                | 11.52 (B)  | 33.09 (B)  | 45.40 (C)  | 87.86 (B)  | 97.75 (T)  | 249.0          | 28.77           |
| 10.80               | 4.32                | 11.61 (B)  | 33.78 (B)  | 46.17 (C)  | 93.66 (B)  | 98.95 (T)  | 245.5          | 29.49           |
| 9.53                | 6.93                | 12.00 (B)  | 31.79 (B)  | 45.62 (C)  | 91.88 (B)  | 96.55 (T)  | 233.7          | 26.47           |
| 9.53                | 5.59                | 12.18 (B)  | 32.85 (B)  | 47.28 (C)  | 91.66 (B)  | 96.91 (T)  | 251.7          | 27.81           |

For the transport airliner  $T_2$  wing, the first five natural frequencies due to the variation of engine mass and its location are presented in Tables 5 and 6, respectively. It should be noted that the transport airliner  $T_2$  has a single engine on each of its wings. Table 5 shows that the first, second and third modes are always bending while the fifth mode is always a coupled mode in bending and torsion. However,

the fourth mode is generally a coupled mode for most of the cases, but when the engine mass is reduced to 25%, the fourth mode although remains a coupled mode, but is dominated by torsion. Table 5 shows that a ±25% alteration of engine mass did not alter the natural frequencies of T2 wing significantly. A small increase or decrease in flutter speed with the alteration of engine mass is also apparent. As was the case with the T<sub>1</sub> wing, the flutter speed for the T<sub>2</sub> wing increases with the increase in engine mass and decreases with the reduction of engine mass. A similar argument based on frequency coalescence relating the separation between the fundamental bending and torsional natural frequencies as given for the T<sub>1</sub> wing, can be applied here to the T<sub>2</sub> wing. In Table 6, the results using engine location variation show that for T<sub>2</sub> wing, significant differences in the modal and flutter characteristics are possible when the engine is moved. For the modal characteristics of T<sub>2</sub>, the first and second modes are always bending dominated, but the corresponding natural frequencies can change up to a maximum of around 10% and 28%, respectively. The third natural frequency can change up to 25% and notably the character of the mode changes from bending to a coupled mode when the engine is moved towards the wing tip, but this mode remains bending as the engine is moved towards the wing root. The fourth mode with a maximum frequency variation of around 25%, changes from a coupled mode to a torsional mode when the engine is moved towards the wing root. By contrast, the fourth mode changes from a coupled mode to a bending mode as the engine is moved towards the wing tip. The fifth mode with maximum possible natural frequency variation of around 20% remains coupled as the engine is moved towards the wing root, but it changes to a bending mode when moved towards the wing tip. For the T<sub>2</sub> wing flutter speed variation of around ±15% is possible by altering the engine position by ±25%.

Table 5 - The effects of the variation of engine mass on the natural frequencies and flutter results of  $T_2$  wing

| Variation             |            |                       | ω <sub>i</sub> (rad/s) |            |                       | Flutter        | Flutter         |  |
|-----------------------|------------|-----------------------|------------------------|------------|-----------------------|----------------|-----------------|--|
| in Engine<br>mass (%) | <i>®</i> 1 | <i>w</i> <sub>2</sub> | <i>0</i> 3             | <i>O</i> 4 | <i>0</i> <sub>5</sub> | speed<br>(m/s) | freq<br>(rad/s) |  |
| -25                   | 19.75 (B)  | 57.27 (B)             | 104.5 (B)              | 121.6 (C)  | 199.7 (C)             | 408.5          | 77.85           |  |
| -20                   | 19.74 (B)  | 56.87 (B)             | 103.5 (B)              | 121.5 (C)  | 199.2 (C)             | 409.3          | 78.00           |  |
| -15                   | 19.73 (B)  | 56.47 (B)             | 102.7 (B)              | 121.3 (C)  | 198.8 (C)             | 409.6          | 78.14           |  |
| -10                   | 19.72 (B)  | 56.08 (B)             | 101.8 (B)              | 121.1 (C)  | 198.4 (C)             | 409.9          | 78.28           |  |
| -5                    | 19.71 (B)  | 55.68 (B)             | 101.0 (B)              | 121.0 (C)  | 198.1 (C)             | 410.2          | 78.43           |  |
| 0                     | 19.71 (B)  | 55.29 (B)             | 100.2 (B)              | 120.9 (C)  | 197.7 (C)             | 410.5          | 78.56           |  |
| 5                     | 19.70 (B)  | 54.90 (B)             | 99.53 (B)              | 120.8 (C)  | 197.4 (C)             | 410.8          | 78.71           |  |
| 10                    | 19.69 (B)  | 54.51 (B)             | 98.84 (B)              | 120.7 (C)  | 197.2 (C)             | 410.9          | 78.83           |  |
| 15                    | 19.68 (B)  | 54.13 (B)             | 98.20 (B)              | 120.7 (C)  | 196.9 (C)             | 411.2          | 78.94           |  |
| 20                    | 19.67 (B)  | 53.76 (B)             | 97.59 (B)              | 120.6 (C)  | 196.6 (C)             | 411.3          | 79.06           |  |
| 25                    | 19.67 (B)  | 53.38 (B)             | 97.01 (B)              | 120.5 (C)  | 196.4 (C)             | 411.5          | 79.18           |  |

Table 6 – The effects of the variation of engine location on the natural frequencies and flutter results of T<sub>2</sub>

| Location of Engine |                       |                       | ω̄ (rad/s) |             |             | Flutter        | Flutter         |
|--------------------|-----------------------|-----------------------|------------|-------------|-------------|----------------|-----------------|
| from wing root (m) | <i>0</i> <sub>1</sub> | <i>0</i> <sub>2</sub> | <i>0</i> 3 | <i>0</i> 04 | <i>0</i> 05 | speed<br>(m/s) | freq<br>(rad/s) |
| 6.41               | 18.50 (B)             | 41.36 (B)             | 75.43 (C)  | 103.9 (B)   | 217.9 (B)   | 344.0          | 72.58           |
| 5.48               | 19.11 (B)             | 44.68 (B)             | 86.04 (C)  | 101.1 (T)   | 215.4 (C)   | 358.0          | 85.84           |
| 5.15               | 19.47 (B)             | 49.18 (B)             | 95.22 (B)  | 104.4 (C)   | 206.3 (C)   | 380.0          | 80.77           |
| 4.37               | 19.71 (B)             | 55.29 (B)             | 100.2 (B)  | 120.9 (C)   | 197.7 (C)   | 410.5          | 78.56           |
| 3.66               | 19.81 (B)             | 59.88 (B)             | 107.5 (B)  | 139.8 (T)   | 194.9 (C)   | 413.5          | 78.85           |
| 2.95               | 19.86 (B)             | 62.64 (B)             | 117.7 (B)  | 160.4 (T)   | 200.5 (C)   | 415.8          | 80.12           |
| 2.22               | 19.88 (B)             | 63.85 (B)             | 125.8 (B)  | 181.8 (T)   | 214.8 (C)   | 416.3          | 81.67           |

For the transport airliner T<sub>3</sub>, the first five natural frequencies due to the variation of engine mass and its location are presented in Tables 7 and 8 respectively. It should be noted that the transport airliner T<sub>3</sub> has a single engine on each of its wings. It can be seen from Table 7 that the natural frequencies are virtually unaltered due to the variation of engine mass. Furthermore, the first, second and third modes are always bending while the fourth and fifth modes are always torsional. The original engine mass corresponding to the unmodified T<sub>3</sub> wing gives the flutter speed as 275 m/s, which is virtually unaltered when changing the engine mass by ±25%. Table 8 shows the results for modal and flutter characteristics when the engine position is altered. As for modal behaviour, it can be seen from this table that the first and the second modes of  $T_3$  are always bending and the fifth mode is always torsional. The third mode changes from bending to coupled and then to torsional as the engine is moved towards the wing root, but it remains bending when it is moved towards the wing tip. The fourth modes change from torsional to coupled and then to bending as the engine is moved towards the wing root. However, the fourth mode remains torsional when the engine is moved towards the wing tip. The flutter speed remains around 275 m/s which in fact corresponds to the case of unmodified T<sub>3</sub> wing, but the flutter speed drops around 9% when the engine is moved towards the tip by 1.6m from its current position. By contrast, when the engine is moved towards the wing root, the flutter speed is virtually unaltered.

Table 7 – The effects of the variation of engine mass on the natural frequencies and flutter results of T<sub>3</sub> wing

| Variation             |                       |                       | ω (rad/s)             |             |                       | Fl. 44 o s                | Flutton                    |
|-----------------------|-----------------------|-----------------------|-----------------------|-------------|-----------------------|---------------------------|----------------------------|
| Engine<br>mass<br>(%) | <i>0</i> <sub>1</sub> | <i>w</i> <sub>2</sub> | <i>w</i> <sub>3</sub> | <i>0</i> 04 | <i>0</i> <sub>5</sub> | Flutter<br>speed<br>(m/s) | Flutter<br>freq<br>(rad/s) |
| -25                   | 12.00 (B)             | 35.08 (B)             | 69.74 (B)             | 72.78 (T)   | 112.5 (T)             | 271.5                     | 44.48                      |
| -20                   | 12.00 (B)             | 34.98 (B)             | 69.27 (B)             | 72.77 (T)   | 112.4 (T)             | 272.5                     | 44.17                      |
| -15                   | 12.00 (B)             | 34.88 (B)             | 68.80 (B)             | 72.76 (T)   | 112.2 (T)             | 273.5                     | 43.88                      |
| -10                   | 11.99 (B)             | 34.78 (B)             | 68.35 (B)             | 72.75 (T)   | 112.0 (T)             | 274.0                     | 43.71                      |
| -5                    | 11.99 (B)             | 34.68 (B)             | 67.90 (B)             | 72.75 (T)   | 111.8 (T)             | 275.0                     | 43.44                      |
| 0                     | 11.99 (B)             | 34.59 (B)             | 67.47 (B)             | 72.74 (T)   | 111.6 (T)             | 275.0                     | 43.16                      |
| 5                     | 11.99 (B)             | 34.49 (B)             | 67.04 (B)             | 72.74 (T)   | 111.5 (T)             | 276.0                     | 43.14                      |
| 10                    | 11.98 (B)             | 34.39 (B)             | 66.63 (B)             | 72.73 (T)   | 111.3 (T)             | 276.5                     | 42.99                      |
| 15                    | 11.98 (B)             | 34.29 (B)             | 66.23 (B)             | 72.73 (T)   | 111.1 (T)             | 277.0                     | 42.87                      |
| 20                    | 11.98 (B)             | 34.19 (B)             | 65.83 (B)             | 72.73 (T)   | 111.0 (T)             | 277.5                     | 42.74                      |
| 25                    | 11.98 (B)             | 34.09 (B)             | 65.45 (B)             | 72.73 (T)   | 110.8 (T)             | 277.5                     | 42.71                      |

Table 8 – The effects of the variation of engine location on the natural frequencies and flutter results of T<sub>3</sub>

| Location                           |            |                       |                       | Flutter     | Flutter     |                |                 |
|------------------------------------|------------|-----------------------|-----------------------|-------------|-------------|----------------|-----------------|
| of Engine<br>from wing<br>root (m) | <i>®</i> 1 | <i>0</i> <sub>2</sub> | <i>დ</i> <sub>3</sub> | <i>0</i> 04 | <i>0</i> 25 | speed<br>(m/s) | freq<br>(rad/s) |
| 5.99                               | 11.83 (B)  | 31.01 (B)             | 63.16 (B)             | 70.09 (T)   | 105.1 (T)   | 257.2          | 36.61           |
| 5.20                               | 11.93 (B)  | 32.98 (B)             | 64.45 (B)             | 71.65 (T)   | 107.8 (T)   | 279.3          | 42.91           |
| 4.40                               | 11.99 (B)  | 34.59 (B)             | 67.47 (B)             | 72.74 (T)   | 111.6 (T)   | 280.0          | 43.16           |
| 3.29                               | 12.02 (B)  | 35.94 (B)             | 72.95 (C)             | 73.95 (C)   | 118.1 (T)   | 284.4          | 42.88           |
| 2.18                               | 12.04 (B)  | 36.47 (B)             | 73.92 (T)             | 77.49 (B)   | 122.1 (T)   | 284.7          | 42.98           |

For the transport airliner  $T_4$ , the first five natural frequencies due to the variation of engine masses and locations are presented in Tables 9 and 10 respectively. It should be noted that the transport airliner  $T_4$  has two engines on each of its wings. Note that, the masses of each of the two engines are increased by the same amount, as indicated in Table 9. Clearly it can be seen from Table 9, that the natural frequencies variation is quite small due to the variation of the engine masses from -25% to +25%. It can also be seen from Table 9 that the first, second and fourth modes are always bending while the third and fifth modes are always torsional within the range of engine mass variation. The changes in natural frequencies and flutter speed due to  $\pm 25\%$  engine mass variations are rather inconsequential. However, the effects of the engine locations on the free vibration and flutter characteristics of  $T_4$  wing shown in Table 10 reveal somehow a different picture for flutter speed when both the inboard and outboard engines are brought nearer to the fuselage and when the outboard engine is moved towards the wing tip. It should be noted that out of all the four aircraft wings analysed, the  $T_4$  wing is the heaviest both in terms of empty wing mass as well as the two engine masses carried by each of the wings. For modal characteristics, the first, second and fourth modes of  $T_4$  wing are always bending while third and fifth modes are always torsional. However, when the outboard engine is moved by only 0.5 m from its

original position towards the wing tip, flutter speed increases by around 20% relative to the flutter speed of the baseline wing.

Table 9 – The effects of the variation of engine mass on the natural frequencies and flutter results of T<sub>4</sub> wing

| Variation             |            |                       | ω̄ (rad/s) |             |            | Flutter        | Flutter         |  |
|-----------------------|------------|-----------------------|------------|-------------|------------|----------------|-----------------|--|
| in Engine<br>mass (%) | <i>0</i> 1 | <i>0</i> <sub>2</sub> | <i>0</i> 3 | <i>0</i> 04 | <i>0</i> 5 | speed<br>(m/s) | freq<br>(rad/s) |  |
| -25                   | 9.324 (B)  | 26.98 (B)             | 45.26 (T)  | 73.25 (B)   | 94.09 (T)  | 386.7          | 46.50           |  |
| -20                   | 9.254 (B)  | 26.86 (B)             | 45.26 (T)  | 73.01 (B)   | 94.09 (T)  | 386.5          | 46.50           |  |
| -15                   | 9.186 (B)  | 26.75 (B)             | 45.26 (T)  | 72.77 (B)   | 94.09 (T)  | 386.3          | 46.50           |  |
| -10                   | 9.118 (B)  | 26.64 (B)             | 45.26 (T)  | 72.54 (B)   | 94.09 (T)  | 386.2          | 46.50           |  |
| -5                    | 9.052 (B)  | 26.54 (B)             | 45.26 (T)  | 72.30 (B)   | 94.09 (T)  | 386.0          | 46.50           |  |
| 0                     | 8.988 (B)  | 26.45 (B)             | 45.26 (T)  | 72.06 (B)   | 94.09 (T)  | 385.8          | 46.50           |  |
| 5                     | 8.924 (B)  | 26.35 (B)             | 45.26 (T)  | 71.83 (B)   | 94.09 (T)  | 385.7          | 46.50           |  |
| 10                    | 8.862 (B)  | 26.26 (B)             | 45.26 (T)  | 71.59 (B)   | 94.09 (T)  | 385.5          | 46.50           |  |
| 15                    | 8.801 (B)  | 26.18 (B)             | 45.26 (T)  | 71.36 (B)   | 94.09 (T)  | 385.5          | 46.50           |  |
| 20                    | 8.741 (B)  | 26.09 (B)             | 45.26 (T)  | 71.13 (B)   | 94.09 (T)  | 385.3          | 46.50           |  |
| 25                    | 8.682 (B)  | 26.01 (B)             | 45.26 (T)  | 70.89 (B)   | 94.09 (T)  | 385.2          | 46.50           |  |

Table 10 – The effects of the variation of engine location on the natural frequencies and flutter results of T<sub>4</sub>

| Engine<br>1 from    | Engine 2 from       |                       |                       | ω <sub>i</sub> (rad/s) |             |                       | Flutter        | Flutter         |
|---------------------|---------------------|-----------------------|-----------------------|------------------------|-------------|-----------------------|----------------|-----------------|
| wing<br>root<br>(m) | wing<br>root<br>(m) | <i>0</i> <sub>1</sub> | <i>w</i> <sub>2</sub> | <i>w</i> <sub>3</sub>  | <i>0</i> 04 | <i>0</i> <sub>5</sub> | speed<br>(m/s) | freq<br>(rad/s) |
| 17.6                | 5.6                 | 8.811 (B)             | 26.69 (B)             | 45.07 (T)              | 70.65 (B)   | 94.31 (T)             | 479.5          | 29.14           |
| 17.6                | 4.6                 | 8.814 (B)             | 26.73 (B)             | 45.08 (T)              | 72.67 (B)   | 94.35 (T)             | 476.6          | 29.20           |
| 17.1                | 7.4                 | 8.972 (B)             | 26.30 (B)             | 45.22 (T)              | 66.62 (B)   | 94.00 (T)             | 389.7          | 46.51           |
| 17.1                | 5.6                 | 8.988 (B)             | 26.45 (B)             | 45.26 (T)              | 72.06 (B)   | 94.09 (T)             | 385.8          | 46.50           |
| 17.1                | 4.6                 | 8.991 (B)             | 26.48 (B)             | 45.28 (T)              | 74.15 (B)   | 94.13 (T)             | 385.8          | 46.50           |
| 15.8                | 7.4                 | 9.400 (B)             | 25.92 (B)             | 45.82 (T)              | 68.11 (B)   | 93.73 (T)             | 433.4          | 42.99           |
| 15.8                | 4.6                 | 9.418 (B)             | 26.08 (B)             | 45.87 (T)              | 72.88 (B)   | 93.82 (T)             | 428.2          | 42.99           |

#### 6. Conclusions

Applying the dynamic stiffness method and Theodorsen type two-dimensional unsteady aerodynamics, the free vibration and flutter characteristics of four transport airliner wings have been investigated. The normal mode method in conjunction with the generalised coordinates has been utilised in formulating the flutter problem. Natural frequencies, mode shapes, flutter speeds and flutter frequencies for the wings are presented and the results are discussed. Next, a detailed parametric study on the effects of the variation of engine mass and location on the free vibration and flutter characteristics has been carried out. The engine masses are varied between +25% and -25% in steps of 5% whereas the engine locations are varied approximately between +2m and -2m in small steps from their current locations depending on the type of the aircraft. The results show that the natural frequencies, mode shapes, flutter speed and flutter frequency can be changed to an appreciable extent for some of the airliner wings to avoid or alleviate aeroelastic problems. Although some of the natural frequency variations due to engine mass and location variations are small, even these small variations could be important to solve frequency attenuation problems and avoid flutter and resonance phenomenon. The investigation provides useful information to aircraft designers to make some engineering judgement on the engine mass and location, from an aeroelastic standpoint. The research carried out here on metallic wings, can be extended to composite wings.

#### 7. Contact Author Email Address

mailto: j.r.banerjee@city.ac.uk

# 8. Copyright Statement

The authors confirm that they, and/or their company or organization, hold copyright on all of the original material included in this paper. The authors also confirm that they have obtained permission, from the copyright holder of any third party material included in this paper, to publish it as part of their paper. The authors confirm that they give permission, or have obtained permission from the copyright holder of this paper, for the publication and distribution of this paper as part of the ICAS proceedings or as individual off-prints from the proceedings.

#### References

- [1] Banerjee J.R. Flutter characteristics of high aspect ratio tailless aircraft, *Journal of Aircraft*, Vol. 21, No. 9, pp 733-736, 1984.
- [2] Banerjee J.R. Flutter modes of high aspect ratio tailless aircraft, *Journal of Aircraft*, Vol. 25, No. 5, pp 473-476, 1988.
- [3] Van Schoor M.C and Von Flotow A.H. Aeroelastic characteristics of a highly flexible aircraft, *Journal of Aircraft*, Vol. 27, No. 10, pp 901-908, 1990.
- [4] Eslimy-Isfahany S.H.R, Banerjee J.R and Sobey A.J. Response of a bending-torsion coupled beam to deterministic and random loads, *Journal of Sound and Vibration*, Vol. 195, No. 2, pp 267-283, 1996.
- [5] Banerjee J.R, Patel M.H, Done G.T.S, Butler R and Lillico M. Free vibration and flutter sensitivity analyses of a large transport aircraft, *Proceedings of the 7th AIAA/USAF/NASA/ISSMO Symposium on Multidisciplinary Analysis and Optimisation*, pp 98-4765, 1998.
- [6] Tang D and Dowell E.H. Experimental and theoretical study on aeroelastic response of high aspect ratio wings, *AIAA Journal*, Vol. 39, No. 8, pp 1430-1441, 2001.

- [7] Banerjee J.R, Liu X and Kassem H.I. Aeroelastic stability of high aspect ratio aircraft wings, *Journal of Applied Nonlinear Dynamics*, Vol. 3, No. 4, pp 413-422, 2014.
- [8] Butler R and Banerjee J.R. Optimum design of bending-torsion coupled beams with frequency or aeroelastic constraints. *Comput Struct*, Vol. 60, pp 715-724, 1996.
- [9] Lillico M, Butler R, Guo S and Banerjee J.R. Aeroelastic optimisation of composite wings using the dynamic stiffness method. *Aeronaut J*, Vol. 101, pp 77-86, 1997.
- [10] Banerjee J.R. The dynamic stiffness method: theory, practice and promise, *Computational Technology Reviews*, Vol. 11, No. 1, pp 3-57, 2015.
- [11] Banerjee J.R. Coupled bending-torsional dynamic stiffness matrix for beam elements, *International Journal for Numerical Methods in Engineering*, Vol. 28, No. 6, pp 1283-1298, 1989.
- [12] Banerjee J.R. A FORTRAN program for computation of coupled bending-torsional dynamic stiffness matrix of beam elements, *Advances in Engineering Software*, Vol. 13, No. 1, pp 17-24, 1991.
- [13] Wittrick W.H and Williams F.W. A general algorithm for computing natural frequencies of elastic structures, *The Quarterly Journal of Mechanics and Applied Mathematics*, Vol. 24, No. 3, pp 263-284, 1971.
- [14] Bisplinghoff R.L, Ashley H and Halfman R.L. Aeroelasticity, Courier Corporation, 2013.
- [15] Banerjee J.R. Use and capability of CALFUN: A program for calculation of flutter speed using normal modes, *Proceedings Int. AMSE Conference on Modelling and Simulation*, Vol. 3, No. 1, pp 121-131, 1984.